

## Article

# Photocatalytically Active Supramolecular Organic-inorganic Magnetic Composites as Efficient Route to Remove $\beta$ -lactam Antibiotics from Water

Sabina Ion <sup>1,2</sup>, Octavian D. Pavel <sup>1,2</sup>, Nicolae Guzo <sup>1,2</sup>, Madalina Tudorache <sup>1,2</sup>, Simona M. Coman <sup>1,2</sup>, Vasile I. Parvulescu <sup>1,2,\*</sup>, Bogdan Cojocaru <sup>1,2,\*</sup> and Elisabeth E. Jacobsen <sup>3,\*</sup>

<sup>1</sup> University of Bucharest, Faculty of Chemistry, 4-12 Regina Elisabeta Av., Bucharest, 030018, Romania

<sup>2</sup> Research Center for Catalysts & Catalytic Processes, Faculty of Chemistry, University of Bucharest, 4-12, Blv. Regina Elisabeta, 030018 Bucharest, Romania

ion.sabina.gabriela@chimie.unibuc.ro (S.I.); octavian.pavel@chimie.unibuc.ro (O.D.P.); nicuguzo@yahoo.com (N.G.); madalina.sandulescu@g.unibuc.ro (M.T.); simona.coman@chimie.unibuc.ro (S.M.C.); vasile.parvulescu@chimie.unibuc.ro (V.I.P.); bogdan.cojocaru@chimie.unibuc.ro (B.C.)

<sup>3</sup> NTNU, Department of Chemistry, Høgskoleringen 5, 7491 Trondheim, Norway  
elisabeth.e.jacobsen@ntnu.no (E.E.J.)

\* Correspondence: vasile.parvulescu@chimie.unibuc.ro (V.I.P.); bogdan.cojocaru@chimie.unibuc.ro (B.C.) and elisabeth.e.jacobsen@ntnu.no (E.E.J.); Tel.: +40213051464 and +4798843559

**Abstract:** Considerable efforts have been made in recent years to identify an optimal treatment method for the removal of antibiotics from wastewaters. A series of supramolecular organic-inorganic magnetic composites containing Zn-modified MgAl LDHs and Cu-phthalocyanine as photosensitizer have been prepared with the scope to  $\beta$ -lactam antibiotics removal from aqueous solutions. The characterization of these materials confirmed the anchorage of Cu-phthalocyanine onto the edges of the LDH lamellae, with a negligible part inserted in the interlayer space. The removal of  $\beta$ -lactam antibiotics occurred via a concerted adsorption and photocatalytic degradation. The efficiency of the composites was depending on *i*) the LDH: magnetic nanoparticle (MP) ratio, that is strongly correlated to the textural properties of the catalysts, and *ii*) the phthalocyanine loading in the final composite. A maximum of the efficiency was achieved with a removal of ~93% of antibiotics after 2h of reaction.

**Keywords:** layered double hydroxides; magnetic nanoparticles; phthalocyanines; antibiotics removal

## 1. Introduction

Antibiotics are by far the most successful class of drugs fighting against the bacterial infections and, therefore, extensively used in both the human and veterinary medicine. These are produced by both microorganisms or via synthetic or semi-synthetic routes where, does not matter of the pathway, the building of the complex chemical structures generates pollutant residues [1]. Besides these, the excretion after their use and the disposal of the un-used medicinal compounds are additional sources of pollution. Some antibiotics, such as penicillins, can be easily degraded, while others, such as fluoroquinolones or tetracyclines, are considerably more persistent. Accordingly, these predominate for a longer time in the environment and accumulate in higher concentrations [1]. Thus, the potential role in promoting the development of a high resistance to human and animal pathogens even enhances the concern about their presence in the environment.

Considerable efforts have been made in recent years to identify an optimal treatment method for the removal of antibiotics from wastewaters. With this aim, advanced oxidation processes (AOP) emerged as a more promising tool compared to more traditional routes, such as the adsorption on activated carbon, air stripping or the reverse osmosis [2]. Indeed, many of these techniques only transfer pollutants from one phase to another

without a complete destruction up to the mineralization. Biological treatment is not toxic to organic culture but has also some limitations [3]. The most important is related to its applicability only for wastewaters containing biodegradable compounds.

Among the various advanced oxidation processes, photocatalysis has emerged as a promising technology for wastewater treatment. The main advantages of the process are the possibility of a simultaneous removal of antibiotics and antibiotic-resistant bacteria, the lack of mass transfer limitations under the operational environmental conditions, and the price, the commercially availability, the non-toxicity and the photochemical stability of the catalyst [4].

Recent research focused organic photocatalysts as mimicking natural supramolecular systems [5] where the triplet states of the excited organic molecule can participate in electron transfer processes quite similar to the semiconductors [5]. Metallophthalocyanines (Pcs) can act as electron donors upon a photochemical excitation in the visible region [5]. However, the use of bare (metallo)phthalocyanines is limited due to the recovery and stability problems [5]. Therefore, their immobilization represents a viable alternative to solve these. TiO<sub>2</sub> immobilized phthalocyanines [6] or mechanical mixtures of metallophthalocyanines and zeolites [5] have already been found effective for the photocatalytic degradation of organic compounds. Encapsulation of these complexes in porous supports led to an increase of the activity compared with the free complex that is the result of two factors: *i*) concentration of substrates around the active sites, and *ii*) a protection against degradation [7].

Encapsulation of metallo-phthalocyanines inside the layered double hydroxides (LDHs) represents another suggested solution to create hybrid organic-inorganic supramolecular systems [8]. In a strong connection to their adsorptive and oxidation catalytic properties, LDHs were utilized in photocatalysis under both UV and Vis light irradiation [9,10]. These studies demonstrated that the immobilization of the macrocyclic complexes may enhance the catalytic behaviour for the environmental pollution control under Vis irradiation, as well, anionic phthalocyanines (sulfonated phthalocyanines) playing the role of the charge neutralizing anion [8,11-16]. However, the conventional catalyst separation methods such as filtration or centrifugation are not always suitable for nanoparticles due to an incomplete separation. To solve this practical problem, magnetic nanoparticles (MNPs) were considered as alternatives. Properties such as high surface areas and chemical stability, non-swelling properties in organic solvents [17], easy recovery by an external magnet, reusability [18], regular shapes, uniform size, low cost of production, non-toxicity and biocompatibility [19] recommend these as catalytic supports.

$\beta$ -Lactam antibiotics such as amoxicillin (AMO), ampicillin (AMP), penicillin G (PEG), penicillin V (PEV) and cloxacillin (CLX) have antimicrobial properties through the presence of a  $\beta$ -lactam ring. These drugs are widely used in medicinal treatments and a high content of their metabolites ends in waste waters, which leads to several negative effects. In accordance, their removal from the environment is imperative, and various procedures involving UV irradiation [20], radiolysis [21], ozonolysis [22], Fenton- and photo-Fenton processes [20,23], photocatalysis with semiconductors [4,24-27], or a combination of these [28] have already been reported. Among these, techniques involving the solar light as source of irradiation in the photodegradation of  $\beta$ -lactam antibiotics are the most appropriate.

In this respect, it was already reported that AMO, AMP, PEV, PEG or CLX can be degraded under visible irradiation by ZnS nanoparticles as a photocatalyst, in a large domain of concentrations (0.5-1000 mg L<sup>-1</sup>), the rate of degradation increasing as the stability of the antibiotic molecules decreased [29]. ZnO nanoparticles and ZnO/polyaniline core-shell nanocomposite also degraded ampicillin under sun-light irradiation [30], while photocatalytic membranes composed of hybrid polylactic acid (PLA)/TiO<sub>2</sub> nanofibers deposited on fiberglass supports exhibited a high rate of degradation of AMP, this being virtually eliminated in the first 30 minutes of process. Also, metallic nanoparticles (Ag-NPs) were used in the photocatalytic degradation of AMP under natural sunlight irradiation with an efficiency of 96.5% [31].

However, in our best knowledge, at least to-date, MPc-LDH-MNP organic-inorganic supramolecular hybrid systems were not investigated as photocatalysts for the removal of  $\beta$ -lactam antibiotics. In accordance, this study reports the preparation of such kind of materials, their characterization and catalytic behaviour for the photodegradation of the  $\beta$ -lactam antibiotics under visible light.

## 2. Results and Discussion

The coding of the catalysts based on their preparation conditions is presented in table 1.

**Table 1.** The preparation details for the catalysts prepared taking different LDH:MNP ratios and from different MNP precursors.

Sample	Precursor	Conditions
P1	FeCl <sub>2</sub> + Fe(NO <sub>3</sub> ) <sub>3</sub>	LDH:Fe <sub>3</sub> O <sub>4</sub> =1:3 (10 min aging)
P2	FeCl <sub>2</sub> + Fe(NO <sub>3</sub> ) <sub>3</sub>	LDH:Fe <sub>3</sub> O <sub>4</sub> =1:3 (30 min aging)
P3	FeCl <sub>2</sub> + Fe(NO <sub>3</sub> ) <sub>3</sub>	LDH:Fe <sub>3</sub> O <sub>4</sub> =3:1 (60 min aging)
P4	FeCl <sub>2</sub> + Fe(NO <sub>3</sub> ) <sub>3</sub>	LDH:Fe <sub>3</sub> O <sub>4</sub> =3:2 (60 min aging)
P5	FeCl <sub>2</sub> + Fe(NO <sub>3</sub> ) <sub>3</sub>	LDH:Fe <sub>3</sub> O <sub>4</sub> =1:1 (60 min aging)
P6	FeCl <sub>2</sub> + Fe(NO <sub>3</sub> ) <sub>3</sub>	LDH:Fe <sub>3</sub> O <sub>4</sub> =1:2 (60 min aging)
P7	FeSO <sub>4</sub> + FeCl <sub>3</sub> (2:1 mol)	LDH:Fe <sub>3</sub> O <sub>4</sub> =3:1 (60 min aging)
P8	FeSO <sub>4</sub> + FeCl <sub>3</sub> (1:2 mol)	LDH:Fe <sub>3</sub> O <sub>4</sub> =3:1 (60 min aging)

### 2.1. Characterization

#### 2.1.1. X-Ray Diffraction (XRD)

As previously reported [32], the X-ray diffractogram of the bare LDH shows, at low angles, narrow and intense diffraction lines and, at high diffraction angles, wide and less intense lines characteristic to the LDH materials [33]. In addition to the lines, the additional ones corresponding to the zincite phase (ZnO) appeared, as minor impurities, in the 2 theta range 31-38°[32]. The reconstruction by memory effect occurred with the preservation of the lines of the stable ZnO phase (ICDD 005-0664).

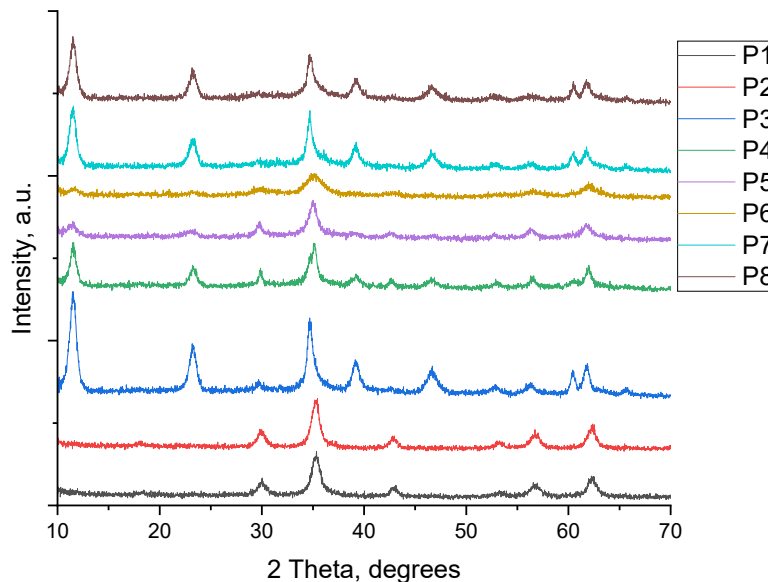


**Figure 1.** X-Ray diffractograms corresponding to P1-P8 catalysts.

The X-ray diffractograms corresponding to P1-P8 catalysts are presented in Figure 1. The magnetite phase can be observed in almost all samples and most predominant for P1,

P2, P5 and P6. Except LDH, Fe<sub>3</sub>O<sub>4</sub> (ICDD 19-0629), and small impurities of ZnO no other phases and impurities were detected.

**Table 2.** Network parameters determined from the X-ray diffractograms for the bare MgZnAl LDH and P1-P8 catalysts.

Sample	a (Å)	c (Å)	IFS (Å) <sup>1</sup>	I <sub>003</sub> /I <sub>006</sub>	I <sub>003</sub> /I <sub>110</sub>	D(Å) <sup>2</sup>
LDH-MgZnAl	3.0717	22.8689	2.82	2.96	5.54	132
P1	3.0462	22.5822	2.73	1.00	0.67	111
P2	3.0557	22.6262	2.74	1.08	0.68	115
P3	3.0616	22.9058	2.84	2.21	4.89	96
P4	3.0539	22.8707	2.82	2.21	6.73	105
P5	3.0644	23.1147	2.90	1.95	4.56	79
P6	3.0663	23.5299	3.04	3.00	1.29	200
P7	3.0612	22.9415	2.85	2.17	3.98	97
P8	3.0589	22.8956	2.83	2.20	4.04	95

<sup>1</sup> IFS represents the distance of the interplanar space (the values using Miyata's reported sheet thickness of 4.8 Å [34]).

<sup>2</sup> The crystallite size (obtained with the Debye-Scherrer equation) and determined from the FWHM value of the reflection 003.

The network parameter "a" (Table 2), calculated as  $a = 2 \cdot d_{110}$  formula, indicating the average cation-cation distance in the layered network, shows a decrease of the inter-layer space, as an effect of hydration associated to the elimination, by calcination, of carbonate anions that are larger and the replacement of these by hydroxyl anions which are much smaller in size. The network parameter "c", calculated as  $c = 3/2 \cdot (d_{003} + 2d_{006})$ , keeps the trend of IFS variation caused by an increase of the electrostatic forces between the layers and the interlayer anions. According to literature the presence of heavy interlayer molecular species led to a change in the electron density of the 001 harmonics, i.e. organic anions [35], metal nanoparticles [36] or oxometalates [37]. Considering the "a" and "c" parameters we can conclude that the majority of phthalocyanine is anchored on the edge of the hydroxide lamellae while a smaller part is placed in the interplanar space. The crystallite size, which in this case is an average of the entire composite, depended on the LDH : MP ratio.

### 2.1.2. Diffuse Reflectance UV-Vis spectroscopy (DR-UV-Vis)

Bare LDH shows a wide absorption band in the range 240 - 380 nm with maxima at 348 and 359 nm, respectively, associated to the presence of zincite in the layered structure [32]. The absorption band at 212 nm corresponds to Mg(OH)<sub>2</sub> / MgO [32,38].

The DR-UV-Vis spectra of the phthalocyanine-LDH composite, exemplified for P2, P3 and P5 catalysts (Figure 2), revealed strong absorption bands in the region 500-900 nm, assigned to their Q bands [39]. Anchoring the magnetic particles led to an additional absorption in the range of 400 - 600 nm [40] that overlaps, in the region 200 - 450 nm, with the absorption bands of MPC [41].

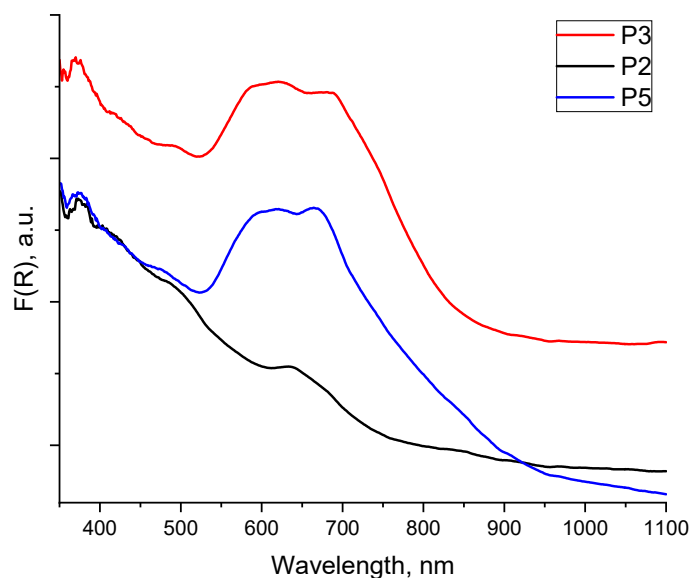


**Figure 2.** DR-UV-VIS spectra collected for P2 (LDH:MP=1:3), P3 (LDH:MP=3:1) and P5 (LDH:MP=1:1) catalysts.

### 2.1.3. Diffuse Reflectance Infrared Spectroscopy (DRIFT)

The intercalation of phthalocyanine was also confirmed by the DRIFT analysis (Figure 3). The wide absorption band located in the  $3700 - 3400 \text{ cm}^{-1}$  range corresponds to the vibrations of the OH,  $\nu(\text{O}-\text{H})$  groups in the interplanar space, while the band at  $3000 \text{ cm}^{-1}$  is assigned the hydrogen bonds between water and the carbonate anion [42]. The band at  $1638 - 1650 \text{ cm}^{-1}$  corresponds to the vibrations of the water molecules in the layered structure, that in the range  $1100$  and  $650 \text{ cm}^{-1}$  to the vibrations of the  $\text{CO}_3^{2-}$  groups and those before  $600 \text{ cm}^{-1}$  to the Mg-O, Zn-O and Al-O bonds. Infrared spectra also showed bands associated to the presence of LDH-anchored phthalocyanine [43]. That at approximately  $1650 \text{ cm}^{-1}$  can be assigned to the C = N bond, that at  $1120 \text{ cm}^{-1}$  to the S = O bond, and those at  $730$ ,  $1033$  and  $1090 \text{ cm}^{-1}$  to the C-H bond.

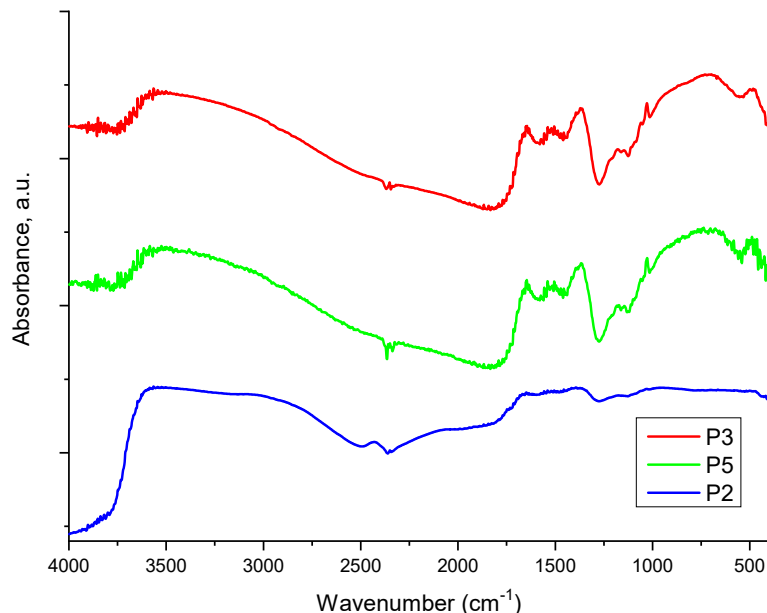


**Figure 3.** DRIFT spectra corresponding to P2 (LDH:MP=1:3), P3 (LDH:MP=3:1) and P5 (LDH:MP=1:1) catalysts.

### 2.1.4. Textural properties

The surface areas of the P1-P8 catalysts (Table 2) varied in a rather narrow range, i.e. from 110 (P4) to 160 m<sup>2</sup>·g<sup>-1</sup> (P5). The increase of the ageing time which means also an increase in the MNP size, led to a decrease of the surface area (samples P1 and P2). All the samples presented a Type IV adsorption-desorption isotherm, characteristic of mesoporous materials (Figure 4). However, depending on the LDH : MNP ratio and the nature of MNP precursors, the variation in the pore size was larger (Table 3, Figure 4).

**Table 3.** Surface area, pore volume and main pore size for P1-P8 catalysts.

Sample	S <sub>s</sub> (BET) (m <sup>2</sup> ·g <sup>-1</sup> )	Pore volume (cm <sup>3</sup> ·g <sup>-1</sup> )	Average pore size (Å)
P1	129	0.277	72
P2	116	0.258	73
P3	137	0.858	34, 317
P4	111	0.392	34, 90, 231
P5	163	0.336	37, 63, 182
P6	148	0.230	36, 45
P7	124	0.628	~200
P8	124	0.498	~200

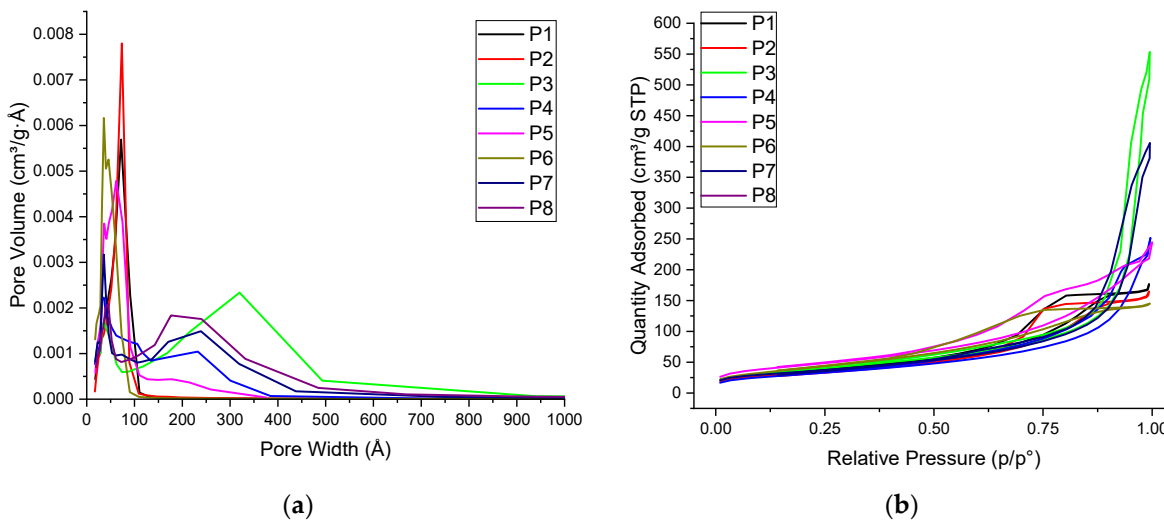


**Figure 4.** Pore size distribution (a) and adsorption-desorption isotherms (b) for the P1-P8 catalysts.

### 2.2. Degradation of Antibiotics

The experiments carried out in this study for the removal of antibiotics from water using the organic-inorganic magnetic composites photocatalysts indicated two parallel processes, namely, the adsorption and the photocatalytic degradation (Figures 5 and 6, respectively).

Simple adsorption measurements indicated a removal of ampicillin in the limits of 9-87%. Considering only this step, the removal of ampicillin varied in the order of efficacy of the photocatalysts: P7>P3>P8>P5>P6>P4>P2~P1 as consequence of their textural properties.

However, the photocatalytic degradation cannot be separated on the adsorption of the ampicillin and degraded fragments, however, it is also depending on the photo-irradiation energy. Under LED irradiation the maximum was achieved for P8, with a removal of ~93% after 2h of reaction. Then, the removal decreased in the order in the order of catalyst used: P7>P5>P8>P3>P6>P4>P2>P1 (Figure 5). The performance of these catalysts depended on the LDH:MNPs ratio and is also related to the textural properties of the composite.

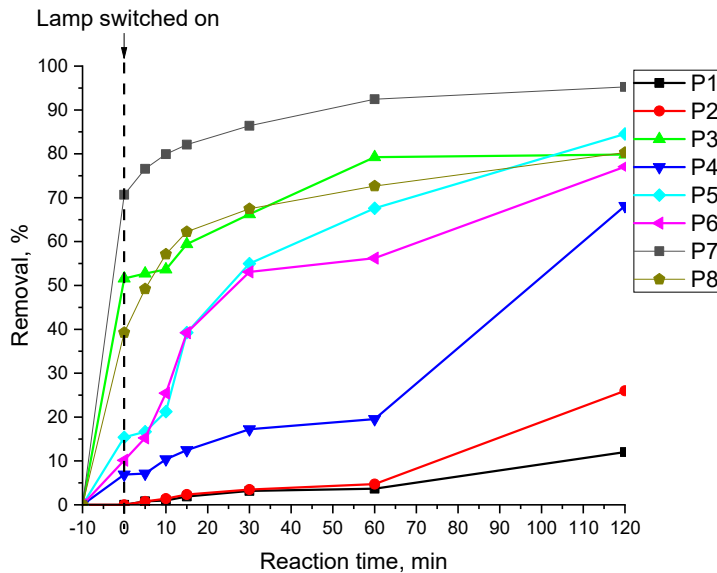


**Figure 5.** Removal of ampicillin from water solution using a blue LED (445-465 nm) as irradiation source.

Moving to a solar simulator as an irradiation source (Figure 6) afforded a higher removal efficiency that is correlated to a higher photocatalytic efficiency assigned to the absorption of the light via the Q bands of phtalocyanine.

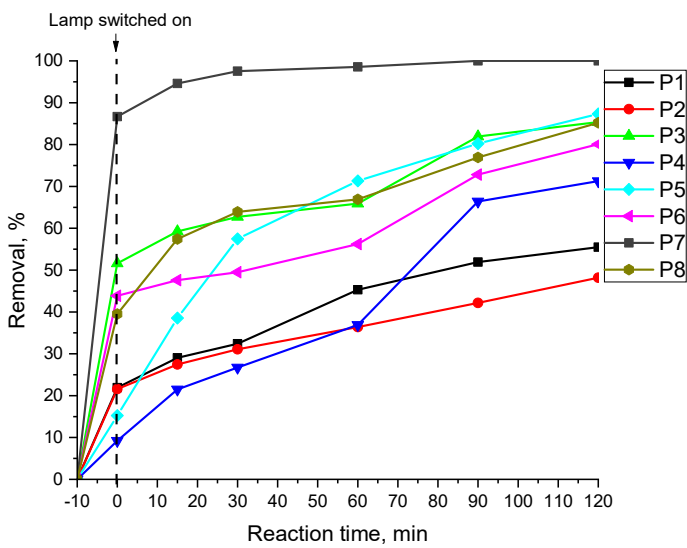


**Figure 6.** Removal of ampicillin from water solution using a solar simulator as irradiation source.

Similar tests in the removal of amoxicillin under solar simulated light irradiation (Figure 7) using selected composites confirmed the order of activity determined for ampicillin. However, both the absorption part and the photocatalytic behavior showed some differences. These are directly related to the structural features of these antibiotics (Figure 8) which can affect both the adsorption of the molecules and the photocatalytic degradation processes. Thus, the degradation of the  $\beta$ -lactam antibiotics can follow two routes, e.g. hydroxylation and opening of the  $\beta$ -lactam ring [44]. The ratio between these routes is influenced by the structure of the antibiotic and the nature of the catalyst. For example, hydroxylation can be enhanced for amoxicillin compared to ampicillin by the population and the strength of the hydroxyl groups able to activate the aromatic ring making it more

susceptible to the attachment of these. However, the mechanism of the photo-degradation of the  $\beta$ -lactam antibiotics is still under discussion.

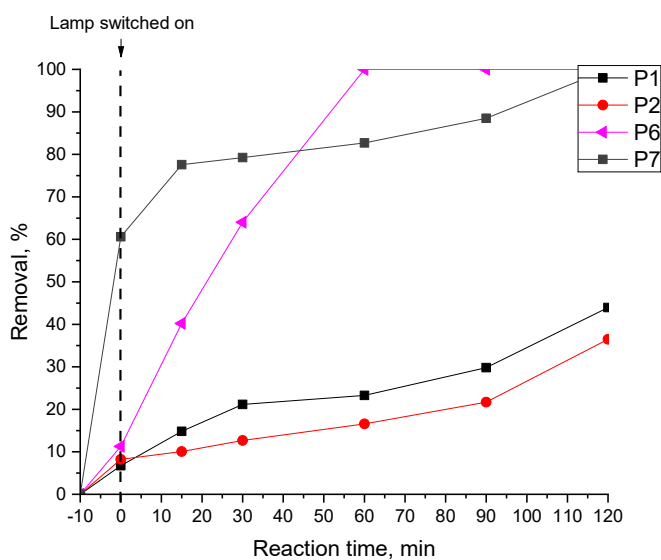


**Figure 7.** Example of removal of amoxicillin from water solution using a solar simulator as an irradiation source.

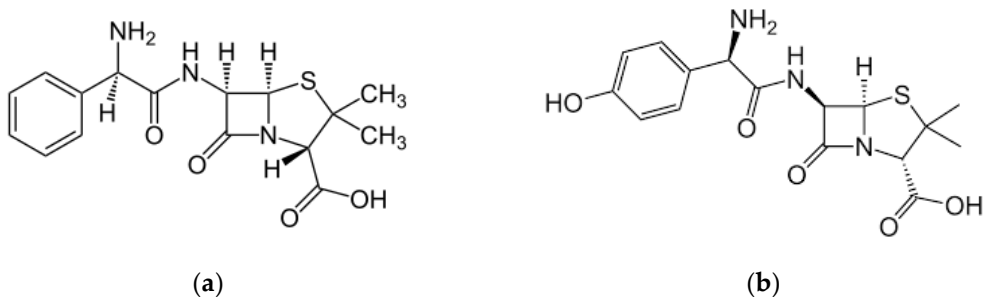


**Figure 8.** Structures of amoxicillin (a) and ampicillin (b).

### 3. Materials and Methods

#### 3.1. Synthesis

The synthesis of LDH  $Mg_{0.375}Zn_{0.375}Al_{0.25}$  has been carried out following a reported procedure [32]. Therefore, two solutions (A and B), were mixed at a inlet flow of  $1\text{ cm}^3\cdot\text{min}^{-1}$ , at RT under stirring (600 rpm). Solution A of a concentration of 1.5M contained the nitrate-like precursors of Mg, Zn and Al in the molar ratio Mg / Zn / Al = 0.375 / 0.375 / 0.25. The base solution contained 0.23 moles NaOH and 0.092 moles  $Na_2CO_3$  at a concentration of 1M in  $Na_2CO_3$ . Co-precipitation of these took place for 1.5 h at the pH of  $10 \pm 0.2$  (continuously monitored by a pH-meter pH315i), after which the resulted precipitate was aged for 18 h, at  $80^\circ\text{C}$  in air atmosphere at the same stirring rate. The suspension was then cooled at room temperature, filtered under vacuum, and washed with distilled water until the pH of 7. The precipitate was dried at  $120^\circ\text{C}$  for 24 h in air atmosphere resulting LDH- $MgZnAl$ . The insertion of phthalocyanine into the structure of LDH started from the calcination of LDH for 18 hours at  $460^\circ\text{C}$  ( $10^\circ\text{C}/\text{min}$ ), then contacting the resulted mixed oxide with a solution of Co-phthalocyanine 3,4',4'',4'''-tetrasulfonic acid (0.1M) under stirring, for 12 h, filtration of the composite phthalocyanine-LDH, washing the precipitate and drying at  $120^\circ\text{C}$  for 24 h in air. The amount of CuPc determined by elemental analysis was  $\sim 10 \times 10^{-5}$  moles CuPc / g of LDH.

The attachment of the magnetic particles (MPs) was achieved by mixing 100 mg of modified LDH with Cu-phthalocyanine in 100 mL of water. After a vigorous stirring for 10 min, the corresponding amounts of  $FeCl_2$  and  $Fe(NO_3)_3$  were added resulting in a

MP@CuPc@LDH-MgZnAl composite. The mixture was then heated at 70 °C on an oil bath and treated, by a slow addition, with 7.5 mL of 5M NaOH. The resulted suspension was then left to aging for 60 min. Finally, the solid was magnetically removed, washed with water by decantation and dried at 70 °C for 12 h.

In order to verify the structural influence of the LDH : MNPs ratio and the nature of the MNP precursors, a series of materials containing CuPc@LDH-MgZnAl were prepared using a similar protocol (Table 1).

### 3.2. Characterization

#### 3.2.1. Specific surface area (BET) and pore size measurements

The investigation of the textural characteristics was performed using the 77K nitrogen adsorption-desorption isotherms collected using a Micromeritics ASAP2020 Surface Area and Porosity Analyzer. The samples were outgassed under vacuum for 24 h at 120 °C.

#### 3.2.2. X-ray Diffraction (XRD)

XRD data were collected at room temperature using a Shimadzu XRD-7000 apparatus taking the monochromatic Cu K $\alpha$  radiation ( $\lambda=1,5406 \text{ \AA}$ , 40 kV, 40 mA), with a scanning rate of 0.1 degrees per minute, in the range  $2\theta = 5 - 80$  degrees.

The size of the crystallites was estimated using Sherrer's equation:

$$D = k \cdot \lambda / FWHM \cdot \sin\theta \quad (1)$$

where:

k = 0.9 (shape factor)

$\lambda$  = wavelength of the X-ray radiation source (for Cu = 1.54  $\text{\AA}$ )

FWHM = full width at half height (in radians)

$\theta$  = maximum position (in radians)

#### 3.2.3. Diffuse Reflectance UV-Vis spectroscopy (DR-UV-Vis)

The DR-UV-Vis spectra were collected under ambient conditions using a Specord 250 equipment (Analytic Jena) with an integrating sphere as measuring device in the reflectance mode. MgO was used as reference material.

#### 3.2.4. Diffuse Reflectance Infrared Spectroscopy (DRIFT)

The infrared spectra were collected with a Brucker Tensor II device equipped with a Harrick Praying Mantis Diffuse Reflection accessory. The final spectra averaged 128 scans with a resolution of 4  $\text{cm}^{-1}$ . KBr was used as a reference.

### 3.3. Photocatalytic tests

The irradiation has been generated by a sunlight simulator using a Luzchem LZC-4b source (LED 445-465 nm), or a Scientech SF150-A Small Collimated Beam Solar Simulator (equipped with Air Mass AM1.5G Filter and Light-Tight Reaction Chamber). The evolution of the photocatalyzed reaction was followed by means of a liquid chromatograph (HPLC) equipped with Zorbax SB-C18 column (4.6 x 150 mm, 5 microns), mobile phase 25 mM KH<sub>2</sub>PO<sub>4</sub>: ACN = 60: 40, mobile phase flow 0.5  $\text{mL} \cdot \text{min}^{-1}$ ; analysis time 30 min; column temperature 60 °C, DAD detection 204 nm). In a typical experiment, 15 mL of a prepared 0.015M solution of antibiotic and 60 mg of catalyst were added into a quartz test-tube. To establish the absorption-desorption equilibrium, before turning on the lamp, the samples were kept in the dark, under stirring, for 10 minutes.

## 4. Conclusions

A series of supramolecular organic-inorganic magnetic composites containing Zn-modified MgAl-LDHs and Cu-phthalocyanine as photosensitizer have been prepared with the scope to  $\beta$ -lactam antibiotics removal from aqueous solutions. The resulted

composites were characterized using textural, spectral and diffractometric techniques. These confirmed the anchorage of Cu-phthalocyanine onto the edges of the LDH lamellae, without any insertion in the interlayer space. The removal of these antibiotics occurred via a concerted adsorption and photocatalytic degradation. The efficiency of the composites was depending on *i*) the LDH:MP ratio that is strongly correlated to the textural properties of the catalysts and *ii*) the phthalocyanine loading in the final composite. A maximum of the efficiency was achieved for the P8 photocatalyst, with a removal of ~93% ampicillin after 2 hours of reaction.

**Author Contributions:** Conceptualization, B.C.; methodology, B.C. and O.D.P.; investigation, S.I., N.G, O.D.P., M.T., S.M.C.; resources, B.C and E.E.J.; writing—original draft preparation, B.C., O.D.P. and E.E.J.; writing—review and editing, V.I.P., B.C., O.D.P. and E.E.J.; supervision, B.C. and M.T.; funding acquisition, M.T. and E.E.J.

All authors have read and agreed to the published version of the manuscript.

**Funding:** This work was financially supported by the Executive Agency for Higher Education, Research, Development and Innovation Funding (UEFISCDI) under Grant PCE 235 and by The Education, Scholarship, Apprenticeships and Youth Entrepreneurship Programmer – EEA Grants 2014–2021, Project No. 18-Cop-0041.

**Data Availability Statement:** The data are available on request from the corresponding author.

**Conflicts of Interest:** The authors declare no conflict of interest.

## References

1. Martinez, J.L. Environmental pollution by antibiotics and by antibiotic resistance determinants. *Environ. Pollut.* **2009**, *157*, 2893–2902, doi:10.1016/j.envpol.2009.05.051.
2. Zhang, G.; Ji, S.; Xi, B. Feasibility study of treatment of amoxillin wastewater with a combination of extraction, Fenton oxidation and reverse osmosis. *Desalination* **2006**, *196*, 32–42, doi:<https://doi.org/10.1016/j.desal.2005.11.018>.
3. Surenjan, A.; Pradeep, T.; Philip, L. Application and performance evaluation of a cost-effective vis- LED based fluidized bed reactor for the treatment of emerging contaminants. *Chemosphere* **2019**, *228*, 629–639, doi:<https://doi.org/10.1016/j.chemosphere.2019.04.179>.
4. Elmolla, E.S.; Chaudhuri, M. Photocatalytic degradation of amoxicillin, ampicillin and cloxacillin antibiotics in aqueous solution using UV/TiO<sub>2</sub> and UV/H<sub>2</sub>O<sub>2</sub>/TiO<sub>2</sub> photocatalysis. *Desalination* **2010**, *252*, 46–52, doi:<https://doi.org/10.1016/j.desal.2009.11.003>.
5. Corma, A.; Garcia, H. Zeolite-based photocatalysts. *Chem. Commun.* **2004** 1443–1459, doi:<https://doi.org/10.1039/B400147H>.
6. Ranjit, K.T.; Willner, I.; Bossmann, S.; Braun, A. Iron(III) phthalocyanine-modified titanium dioxide: A novel photocatalyst for the enhanced photodegradation of organic pollutants. *J. Phys. Chem. B* **1998**, *102*, 9397–9403, doi:10.1021/jp982694s.
7. Zsigmond, A.; Notheisz, F.; Bäckvall, J.-E. Rate enhancement of oxidation reactions by the encapsulation of metal phthalocyanine complexes. *Catal. Lett.* **2000**, *65*, 135–139, doi:<https://doi.org/10.1023/A:1019005018899>.
8. Perez-Bemal, E.; Ruano-Casero, R.; Pinnavaia, T.J. Catalytic autoxidation of 1-decanethiol by cobalt(II) phthalocyaninetetrasulfonate intercalated in a layered double hydroxide. *Catal. Lett.* **1991**, *11*, 55, doi:<https://doi.org/10.1007/BF00866901>.
9. Mohapatra, L.; Parida, K. A review on the recent progress, challenges and perspective of layered double hydroxides as promising photocatalysts. *Mater. Chem. A* **2016**, *4*, 10744, doi:<https://doi.org/10.1039/C6TA01668E>.
10. Gao, L.-G.; Gao, Y.-Y.; Song, X.-L.; Ma, X.-R. A novel La<sup>3+</sup>-Zn<sup>2+</sup>-Al<sup>3+</sup>-MoO<sub>4</sub><sup>2-</sup> layered double hydroxides photocatalyst for the decomposition of dibenzothiophene in diesel oil. *Pet. Sci. Technol.* **2008**, *0*, 1–6, doi:<https://doi.org/10.1080/10916466.2018.1447957>.
11. Barbosa, C.A.S.; Ferrira, A.M.D.C.; Constantino, V.R.L.; Coelho, A.C.V. Preparation and Characterization of Cu(II) Phthalocyanine Tetrasulfonate Intercalated and Supported on Layered Double Hydroxides. *J. Incl. Phenom. Macro. Chem.* **2002**, *42* 15, doi:<https://doi.org/10.1023/A:1014598231722>.
12. Barbosa, C.A.S.; Dias, P.M.; Ferrira, A.M.C.; Constantino, V.R.L. Mg-Al hydrotalcite-like compounds containing iron-phthalocyanine complex: effect of aluminum substitution on the complex adsorption features and catalytic activity. *Appl. Clay. Sci.* **2005**, *28* 147, doi:<https://doi.org/10.1016/j.clay.2004.02.002>.
13. Barbosa, C.A.S.; Ferrira, A.M.D.C.; Constantino, V.R.L. Synthesis and Characterization of Magnesium-Aluminum Layered Double Hydroxides Containing (Tetrasulfonated porphyrin)cobalt. *Eur. J. Inorg. Chem.* **2005**, *1577*, doi:<https://doi.org/10.1002/ejic.200400875>.
14. Kanan, S.; Awate, S.V.; Agashe, M.S. Incorporation of anionic copper phthalocyanine complexes into the intergallery of Mg-Al layered double hydroxides. *Stud. Surf. Sci. Catal.* **1998**, *113* 927, doi:[https://doi.org/10.1016/S0167-2991\(98\)80380-7](https://doi.org/10.1016/S0167-2991(98)80380-7).
15. Parida, K.M.; Baliarsingh, N.; Sairam Patra, B.; Das, J. Copperphthalocyanine immobilized Zn/Al LDH as photocatalyst under solar radiation for decolorization of methylene blue. *J. Mol. Catal. A: Chemical* **2007**, *267* 202–208, doi:<https://doi.org/10.1016/j.molcata.2006.11.035>.

16. Maretti, L.; Carbonell, E.; Alvaro, M.; Scaiano, J.C.; Garcia, H. Laser flash photolysis of dioxo iron phthalocyanine intercalated in hydrotalcite and its use as a photocatalyst. *J. Photochem. Photobio. A: Chemistry* **2009**, *205*, 19-22, doi:<https://doi.org/10.1016/j.jphotochem.2009.04.006>.
17. Abu-Reziq, R.; Alper, H.; Wang, D.; Post, M.L. Metal Supported on Dendronized Magnetic Nanoparticles: Highly Selective Hydroformylation Catalysts. *J. Am. Chem. Soc.* **2006**, *128*, 5279-5282, doi:<https://doi.org/10.1021/ja060140u>.
18. Karaoglu, E.; Baykal, A.; Erdemi, H.; Alpsoy, L.; Sozeri, H. Synthesis and characterization of dl-thiocit acid (DLTA)-Fe<sub>3</sub>O<sub>4</sub> nanocomposite. *J. Alloys Compd.* **2011**, *509*, 9218-9225, doi:<https://doi.org/10.1016/j.jallcom.2011.06.118>.
19. Naeimi, H.; Nazifi, Z.S. A highly efficient nano-Fe<sub>3</sub>O<sub>4</sub> encapsulated-silica particles bearing sulfonic acid groups as a solid acid catalyst for synthesis of 1,8-dioxo-octahydroxanthene derivatives. *J. Nanopart. Res.* **2013**, *15*, 2026-2032, doi:<https://doi.org/10.1007/s11051-013-2026-2>.
20. Brillas, E. A review on the photoelectro-Fenton process as efficient electrochemical advanced oxidation for wastewater remediation. Treatment with UV light, sunlight, and coupling with conventional and other photo-assisted advanced technologies. *Chemosphere* **2020**, *250*, 126198, doi:<https://doi.org/10.1016/j.chemosphere.2020.126198>.
21. Szabó, L.; Tóth, T.; Engelhardt, T.; Rácz, G.; Mohácsi-Farkas, S.; Takács, E.; Wojnárovits, L. Change in hydrophilicity of penicillins during advanced oxidation by radiolytically generated OH compromises the elimination of selective pressure on bacterial strains. *Sci. Total Environ.* **2016**, *551-552*, 393-403, doi:<https://doi.org/10.1016/j.scitotenv.2016.02.002>.
22. Andreozzi, R.; Canterino, M.; Marotta, R.; Paxeus, N. Antibiotic removal from wastewaters: The ozonation of amoxicillin. *J. Hazard. Mater.* **2005**, *122*, 243-250, doi:<https://doi.org/10.1016/j.jhazmat.2005.03.004>.
23. Rozas, O.; Contreras, D.; Mondaca, M.A.; Pérez-Moya, M.; Mansilla, H.D. Experimental design of Fenton and photo-Fenton reactions for the treatment of ampicillin solutions. *J. Haz. Mat.* **2010**, *177*, 1025-1030, doi:<https://doi.org/10.1016/j.jhazmat.2010.01.023>.
24. Belhacova, L.; Bibova, H.; Marikova, T.; Kuchar, M.; Zouzelka, R.; Rathousky, J. Removal of Ampicillin by Heterogeneous Photocatalysis: Combined Experimental and DFT Study. *Nanomater.* **2021**, *11*, 1992, doi:<https://doi.org/10.3390/nano11081992>.
25. Dimitrakopoulou, D.; Rethemiotaki, I.; Frontistis, Z.; Xekoukoulotakis, N.P.; Venieri, D.; Mantzavinos, D. Degradation, mineralization and antibiotic inactivation of AMX by UV-A/TiO<sub>2</sub> photocatalysis. *J. Environ. Manag.* **2012**, *98*, 168-174, doi:<https://doi.org/10.1016/j.jenvman.2012.01.010>.
26. Klauson, D.; Babkina, J.; Stepanova, K.; Krichevskaya, M.; Preis, S. Aqueous photocatalytic oxidation of amoxicillin. *Catal. Today* **2010**, *151*, 39-45, doi:<https://doi.org/10.1016/j.cattod.2010.01.015>.
27. Shaykhi, Z.M.; Zinatizadeh, A.A.L. Statistical modeling of photocatalytic degradation of synthetic AMX wastewater in an immobilized TiO<sub>2</sub> photocatalytic reactor using response surface methodology. *J. Taiwan Inst. Chem. Eng.* **2014**, *45*, 1717-1726, doi:<https://doi.org/10.1016/j.jtice.2013.12.024>.
28. Hou, J.; Chen, Z.; Gao, J.; Xie, Y.; Li, L.; Qin, S.; Wang, Q.; Mao, D.; Luo, Y. Simultaneous removal of antibiotics and antibiotic resistance genes from pharmaceutical wastewater using the combinations of up-flow anaerobic sludge bed, anoxic-oxic tank, and advanced oxidation technologies. *Water Res.* **2019**, *159*, 511-520, doi:<https://doi.org/10.1016/j.watres.2019.05.034>.
29. Pouretedala, H.R.; Hasanali, M.A. Photocatalytic degradation of some b-lactam antibiotics in aqueous suspension of ZnS nanoparticles. *Desalination Water Treat.* **2013**, *51*, 2617-2623, doi:<https://doi.org/10.1080/19443994.2012.749197>.
30. Nosrati, R.; Olad, A.; Maramifar, R. Degradation of ampicillin antibiotic in aqueous solution by ZnO/polyaniline nanocomposite as photocatalyst under sunlight irradiation. *Environ. Sci. Pollut. Res.* **2012**, *19*, 2291-2299, doi:<https://doi.org/10.1007/s11356-011-0736-5>.
31. Jassal, P.S.; Khajuria, R.; Sharma, R.; Debnath, P.; Verma, S.; Johnson, A.; Kumar, S. Photocatalytic degradation of ampicillin using silver nanoparticles biosynthesised by Pleurotus ostreatus. *BioTechnologia* **2020**, *101*, 5-14, doi:<https://doi.org/10.5114/bta.2019.90246>.
32. Zăvoianu, R.; Mihăilă, S.-D.; Cojocaru, B.; Tudorache, M.; Parvulescu, V.I.; Pavel, O.D.; Oikonomopoulos, S.; Jacobsen, E.E. An advanced approach for MgZnAl-LDH catalysts synthesis used in Claisen-Schmidt condensation. *Catalysts* **2022**, *12*, 759, doi:<https://doi.org/10.3390/catal12070759>.
33. Pavel, O.D.; Stamate, A.-E.; Zăvoianu, R.; Bucur, I.C.; Bîrjega, R.; Angelescu, E.; Pârvulescu, V.I. Mechano-chemical versus co-precipitation for the preparation of Y-modified LDHs for cyclohexene oxidation and Claisen-Schmidt condensations. *Appl. Catal. A, General* **2020**, *605*, 117797, doi:<https://doi.org/10.1016/j.apcata.2020.117797>.
34. Miyata, S. The Syntheses of Hydrotalcite-Like Compounds and Their Structures and Physico-Chemical Properties—I: the Systems Mg<sup>2+</sup>-Al<sup>3+</sup>-NO<sub>3</sub><sup>-</sup>, Mg<sup>2+</sup>-Al<sup>3+</sup>-Cl<sup>-</sup>, Mg<sup>2+</sup>-Al<sup>3+</sup>-ClO<sub>4</sub><sup>-</sup>, Ni<sup>2+</sup>-Al<sup>3+</sup>-Cl<sup>-</sup> and Zn<sup>2+</sup>-Al<sup>3+</sup>-Cl<sup>-</sup>. *Clays Clay Miner.* **1975**, *23*, 369-375, doi:<https://doi.org/10.1346/CCMN.1975.0230508>.
35. Prévot, V.; Casala, B.; Ruiz-Hitzky, E. Intracrystalline alkylation of benzoate ions into layered double hydroxides. *J. Mater. Chem.* **2001**, *11*, 554-560, doi:<https://doi.org/10.1039/B004954I>.
36. Mastalir, Á.; Király, Z. Pd nanoparticles in hydrotalcite: mild and highly selective catalysts for alkyne semihydrogenation. *J. Catal.* **2003**, *220*, 372-381, doi:[https://doi.org/10.1016/S0021-9517\(03\)00269-0](https://doi.org/10.1016/S0021-9517(03)00269-0).
37. Carja, G.; Delahay, G. Mesoporous mixed oxides derived from pillared oxovanadates layered double hydroxides as new catalysts for the selective catalytic reduction of NO by NH<sub>3</sub>. *Appl. Catal. B, Environmental* **2004**, *47*, doi:<https://doi.org/10.1016/j.apcatb.2003.07.004>.

- 
38. Yousefi, S.; Ghasemi, B.; Tajally, M.; Asghari, A. Optical properties of MgO and Mg(OH)<sub>2</sub> nanostructures synthesized by a chemical precipitation method using impure brine. *J. Alloys Compd.* **2017**, *711*, 521-529, doi:<https://doi.org/10.1016/j.jallcom.2017.04.036>.
39. Sakamoto, K.; Ohno-Okumura, E. Syntheses and Functional Properties of Phthalocyanines. *Materials* **2009**, *2*, 1127-1179, doi:<https://doi.org/10.3390/ma2031127>.
40. Rajendran, K.; Balakrishnan, G.S.; Kalirajan, J. Synthesis of Magnetite Nanoparticles for Arsenic Removal from Ground Water Pond. *Int. J. PharmTech Res.* **2015**, *8*, 670-677.
41. Zhang, C.; Tong, S.W.; Jiang, C.; Kang, E.T.; Chan, D.S.H.; Zhu, C. Simple tandem organic photovoltaic cells for improved energy conversion efficiency. *Appl. Phys. Lett.* **2008**, *92*, 68, doi:<https://doi.org/10.1063/1.2885721>.
42. Pavel, O.D.; Zăvoianu, R.; Bîrjega, R.; Angelescu, E.; Pârvulescu, V.I. Mechanochemical versus co-precipitated synthesized lanthanum-doped layered materials for olefin oxidation. *Appl. Catal. A, General* **2017**, *542*, 10-20, doi:<https://doi.org/10.1016/j.apcata.2017.05.012>.
43. Huang, F.; Tian, S.; Qi, Y.; Li, E.; Zhou, L.; Qiu, Y. Synthesis of FePcS-PMA-LDH Cointercalation Composite with Enhanced Visible Light Photo-Fenton Catalytic Activity for BPA Degradation at Circumneutral pH. *Materials* **2020**, *13*, 1951, doi:<https://doi.org/10.3390/ma13081951>.
44. Dogan, S.; Kidak, R. A Plug flow reactor model for UV-based oxidation of amoxicillin. *Desalination Water Treat.* **2016**, *57*, 13586-13599, doi:<https://doi.org/10.1080/19443994.2015.1058728>.